Developing active manipulators in aircraft flight control

Fu, Wei; Van Paassen, M. M.; Mulder, Max

DOI
10.2514/1.G004186

Publication date
2019

Document Version
Final published version

Published in
Journal of Guidance, Control, and Dynamics

JOURNAL OF GUIDANCE, CONTROL, AND DYNAMICS
Vol. 42, No. 8, August 2019

Developing Active Manipulators in Aircraft Flight Control

Wei Fu,* M. M. Van Paassen,† and Max Mulder‡
Delft University of Technology, 2600 GB Delft, The Netherlands

DOI: 10.2514/1.G004186

Most haptic interfaces developed for aircraft control provide haptic support as an additional force on the control manipulator. This study revisits the active manipulator, which is a design concept that is different from but complementary to existing haptic interfaces. This control device sends the force that the pilot exerts on it to the aircraft while feeding back the aircraft rotational rate by means of its deflection angle. It is found that, in comparison with the conventional passive manipulator, the active manipulator greatly facilitates target following and disturbance rejection in compensatory tracking tasks. Furthermore, larger improvements in task performance are associated with higher forcing-function bandwidths. These findings are accounted for by the fact that the active manipulator changes the effective controlled-element dynamics into integratorlike dynamics while at the same time integrating disturbance rejection into the neuromuscular system. However, the high-frequency disturbances acting on the aircraft present in feedback about the aircraft state adversely affect the operational effectiveness of the active manipulator. Based on the experimental findings and results from the passivity theory, a lead–lag filter is designed and evaluated, which mitigates this effect without affecting task performance.

Nomenclature

A	=	amplitude of the sinusoidal component of the forcing function, rad
$b_{m,p}$	=	damping constant of the passive manipulator, $(\mathrm{N}\cdot\mathrm{m}\cdot\mathrm{s})/\mathrm{rad}$
e	=	tracking error, deg
f_d	=	disturbance forcing function, rad
f_m	=	pilot's torque, $\mathrm{N}\cdot\mathrm{m}$
f_t	=	target forcing function, rad
f_d^*	=	adapted disturbance forcing function, rad
H_{CL}	=	closed-loop dynamics of the overall system
H_c	=	dynamics of the controlled element
$H_{c,\mathrm{eff}}$	=	dynamics of the effective controlled element for the active manipulator
H_e	=	dynamics of the pilot's response to the visual error
H_{lpf}	=	dynamics of the low-pass filter used for the active manipulator
$H_{m,a}$	=	dynamics of the active manipulator
$H_{m,\mathrm{af}}$	=	dynamics of the active manipulator with the lead–lag filter
$H_{m,p}$	=	dynamics of the passive manipulator
H_{OL}	=	open-loop dynamics of the overall system
H_x	=	dynamics of the pilot's response to the manipulator movement
K_c	=	controlled-element gain
K_f	=	forward gain of the aircraft control loop
K_m	=	gain of the servo system of the active manipulator
$k_{m,p}$	=	spring constant of the passive manipulator, $(\mathrm{N}\cdot\mathrm{m})/\mathrm{rad}$
$m_{m,p}$	=	inertia constant of the passive manipulator, $\mathrm{kg}\cdot\mathrm{m}^2$
s	=	Laplace variable
u_p	=	pilot control signal
x_m	=	manipulator deflection angle, rad
ζ_{lpf}	=	damping ratio of the low-pass filter of the active manipulator
ϕ	=	roll angle, rad
ϕ_m	=	phase margin, deg
$\dot{\phi}$	=	roll rate, rad/s
ω	=	frequency, rad/s
ω_c	=	crossover frequency, rad/s
$\omega_{\mathrm{lpf},L}$	=	lead corner frequency of the low-pass filter of the active manipulator, rad/s
$\omega_{\mathrm{lpf},l}$	=	lag corner frequency of the low-pass filter of the active manipulator, rad/s

Subscripts

d	=	disturbance rejection
t	=	target following

Presented as Paper 2019-1231 at the AIAA Science and Technology Forum and Exposition (AIAA SciTech 2019), San Diego, CA., 7–11 January 2019; received 29 October 2018; revision received 21 January 2019; accepted for publication 24 January 2019; published online 15 March 2019.

*Ph.D. Student, Section Control and Simulation, Faculty of Aerospace Engineering; w.fu-1@tudelft.nl. Student Member AIAA.

†Associate Professor, Section Control and Simulation, Faculty of Aerospace Engineering; m.m.vanpaassen@tudelft.nl. Member AIAA.

‡Full Professor, Section Control and Simulation, Faculty of Aerospace Engineering; m.mulder@tudelft.nl. Associate Fellow AIAA.

I. Introduction

IN RECENT years, haptic interfaces have received increased interest and facilitated manual control task innovations in many fields, such as surgical robots, terrestrial and space operations, as well as nuclear plant operations [1–7]. In general, a haptic interface is established with a control manipulator, through which a human operator exerts control while haptically receiving information about the controlled system.

In contrast to the conventional aircraft control, in which the pilot controls the aircraft through a passive manipulator and only receives information about the aircraft states through the vision and motion sensory systems, a haptic interface can introduce additional ways to inform the pilot. The fly-by-wire system of modern aircraft offers the possibility to design the control manipulator as a haptic interface, thereby establishing bilateral transmission of information and facilitating manual aircraft control. In general, existing haptic interfaces developed for aircraft control work as support systems that inform the pilot about one or more aspects, such as the current flight condition, the task, or constraints (e.g., boundaries or dangers) in the environment. The common approach taken is by providing additional forces commanded by a haptic support system [7,8]. However, the manipulator itself is still a passive device with its own dynamics, decoupled from those of the aircraft. Due to this, a direct connection between the pilot and the aircraft is not fully established.

Apart from the haptic support systems, there is still much room for improvement on the manipulator itself. To this end, in this study, we fundamentally change the nature of the manipulator. The current work draws primarily on the foundation laid by previous attempts by Hosman et al. [9] and Hosman and Van der Vaart [10], in which the

active manipulator was developed. The active manipulator is based on the admittance display architecture [11], in which a particular state of the controlled aircraft (in our case, the attitude rate) is displayed through the movement of the control manipulator. The pilot's control input to the aircraft, in this case, is derived from the force applied to the manipulator (see Sec. II for more details). In this way, the manipulator is completely coupled to the aircraft.

It was demonstrated that the prototype of the active manipulator led to considerable improvements in the flight control performance [9,10]. However, knowledge about the guiding principle that accounts for such improvements is still lacking, largely impeding attempts at further development of the active manipulator. In this study, an investigation was conducted first to allow for corroboration of the previous findings, as well as to gather theoretical evidence that supports those findings. To this end, an experiment in which participants performed compensatory tasks with various forcing-function bandwidths was carried out. Second, we found that the control task was facilitated by only the feedback of a certain low-frequency segment of the power spectrum of the aircraft state. Due to the disturbance (e.g., turbulence) acting on the aircraft, the feedback beyond this frequency range actually reduced the operational quality of the active manipulator. A lead–lag filter was designed to selectively decouple the dynamics of the active manipulator from those of the aircraft. The viability of the filter was then proven by the control task in a second experiment.

This paper is organized as follows: Sec. II elaborates on the design principle behind the active manipulator. The setup of the first experiment that compares the active and passive manipulators in addition to the analysis of the result are given in Secs. III and IV, respectively. The principle behind the pilot's performance improvement associated with the active manipulator is revealed in Sec. V. Section VI presents the design of a lead–lag filter to improve performance, the tuning of which was tested experimentally as discussed in Sec. VII. The contributions of this study are discussed and summarized in Secs. VIII and IX.

II. Active Manipulator

In conventional aircraft control, the pilot controls the aircraft by means of the deflection angle of a passive manipulator. For instance, consider the control of the aircraft roll angle, as can be seen in Fig. 1a. The passive manipulator usually resembles a mass–spring–damper system. Changing the manipulator deflection angle x_m resembles moving a mass that is connected with a spring and a damper to an infinitely stiff basis. However, due to the aircraft dynamics, the manipulator movement is different than the aircraft's and does not reflect any of the true aircraft states. The pilot can only perceive the information about the aircraft states through vision and motion.

In addition to other sensory channels, the active manipulator involves the haptic channel in perceiving the aircraft's state information. It allows the pilot to directly perceive an aircraft output (typically the aircraft rotational velocity) through the manipulator. Figure 1b shows an example of the control of the aircraft roll angle. As can be seen, the force f_m that the pilot applies on the manipulator is measured and fed to the aircraft. At the same time, the manipulator deflection is driven by a position servo system, which tracks the angular velocity of the aircraft $\dot{\phi}$. If we ignore the dynamics of the force sensor and servo system, the deflection of the active manipulator x_m is proportional to $\dot{\phi}$: $x_m = K_m\dot{\phi}$.

As compared to the passive manipulator, the active manipulator leads to significant improvements in flight control performance [9,10]. However, as mentioned earlier, these findings lack a theoretical basis. Hence, to obtain more insights, as well as to provide a comparison with previous results, we conducted an experiment, which is discussed in the next section.

III. Experiment One: Effects of the Active Manipulator on Human Control Behavior

A roll-axis compensatory task, which involves both target following and disturbance rejection, is performed. The two manipulator types (namely, the active and passive manipulators) are compared in terms of the task performance. The target and disturbance signals are designed with three different bandwidths to evaluate the active manipulator in cases of different task difficulties. A factorial combination of the two manipulator types and the three forcing-function bandwidths yields six experimental conditions. Twelve subjects participated in the experiment. To ensure stable performance, extensive training was performed before the measurements were collected. The remainder of this section gives details about the experiment.

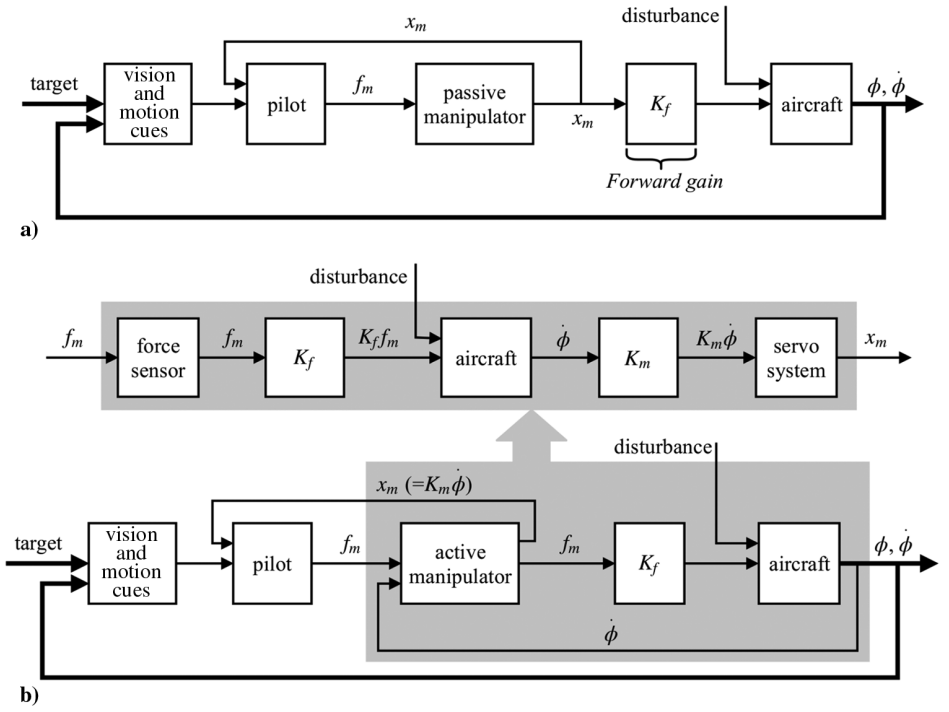

Fig. 1 Schematic diagrams of the control of the aircraft roll attitude with a) the passive manipulator; and b) the active manipulator.

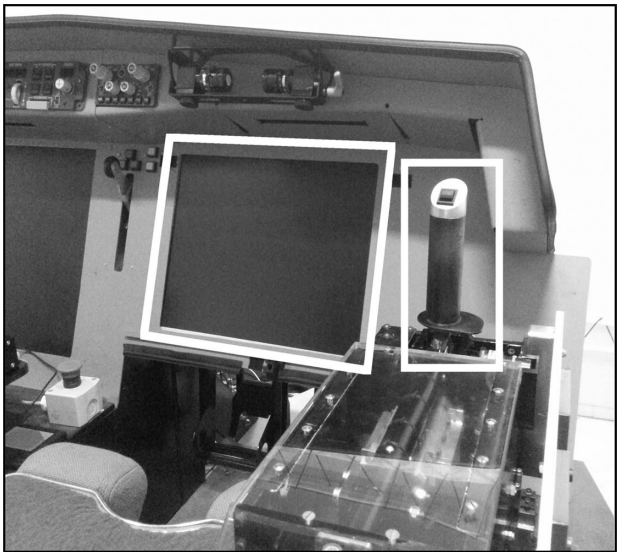

Fig. 2 Devices used for the experiment.

A. Apparatus

The visual display (an Liquid Crystal Display screen) and the manipulator used for the experiment are marked by white boxes in Fig. 2. The manipulator is a control loading device that is equipped with a force sensor and driven by an electrohydraulic position servo system with a bandwidth of around 40 Hz. Such a device allows for the realization of both passive and active manipulators. The manipulator is supplied with a handle (with a diameter of 35 mm) with grooves for placement of the fingers. When a hand is correctly placed on the handle, the center of the hand lies 90 mm above the manipulator rotation axis. During the experiment, the manipulator movement around the pitch axis (fore/aft) is fixed at the neutral position. The range of travel with respect to the roll axis is limited to ± 0.47 rad.

B. Setup of the Compensatory Task

Figures 3a and 3b, respectively, illustrate the compensatory tasks with the two manipulator types. Please note that, except for the manipulator setup and u_p (the output of the manipulator), the tasks with the two manipulator types are exactly the same. The task requires the pilot to minimize the tracking error e, the difference between the target forcing function f_t, and the controlled-element

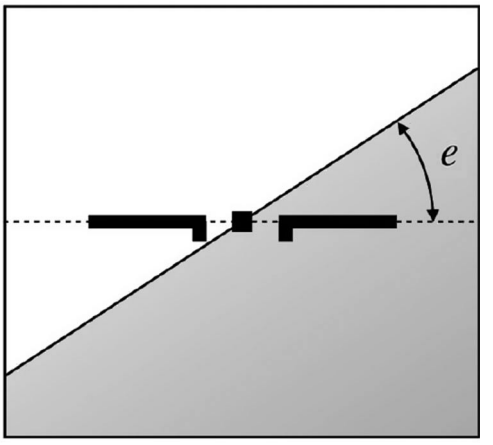

Fig. 4 Simplified artificial horizon.

output ϕ: $e = f_t - \phi$. In the experiment, e is presented on the visual display with a simplified artificial horizon indicator, as can be seen from Fig. 4.

The pilot generates the control signal u_p using the manipulator, on the basis of the visually perceived e. Here, u_p is different between the two manipulator types. For the passive manipulator, u_p is the manipulator deflection angle: $u_p = x_m$. The shaded area in Fig. 3a gives a simplified diagram of how the passive manipulator is realized using our control loading device.

In this study, the dynamics of a linear mass–spring–damper system are used as the desired dynamics of the passive manipulator:

$$H_{m,p}(s) = \frac{X_m(s)}{F_m(s)} = \frac{1}{m_{m,p}s^2 + b_{m,p}s + k_{m,p}} \tag{1}$$

In this study, we ignore the effect of the force sensor and the servo system; therefore, the realized manipulator dynamics are considered to be the same as the desired dynamics $H_{m,p}$. Table 1 lists the mass, damping, and stiffness properties of the passive manipulator. Please note that all the mechanical properties are expressed in the rotational coordinate system, and the corresponding linear values can be derived using the distance from the effective grip point to the axis of rotation (90 mm; see Sec. III.A).

In the case of the active manipulator, the control signal u_p equals the force f_m that the pilot exerts on the manipulator: $u_p = f_m$.

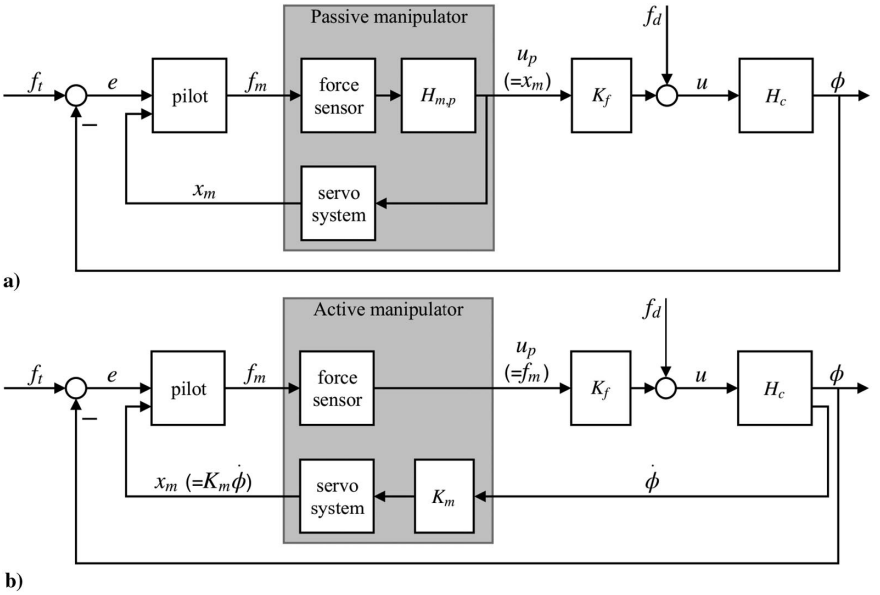

Fig. 3 Schematic diagrams of the compensatory task a) with the passive manipulator; and b) with the active manipulator.

Table 1 Dynamic properties of the passive manipulator

Parameter	Value
$m_{m,p}$, kg/m^2	0.012
$b_{m,p}$, (N · m · s)/rad	0.2
$k_{m,p}$, (N · m)/rad	2.0

Table 2 The corner frequencies of the magnitudes of the forcing functions

Bandwidth	$\omega_{\mathrm{ff},l}$, rad/s	$\omega_{\mathrm{ff},L}$, rad/s
BW1	0.60	4.80
BW2	1.00	8.00
BW2	1.65	13.2

The shaded area in Fig. 3b shows how the active manipulator is implemented. As mentioned earlier, the manipulator deflection x_m is proportional to the aircraft rotational velocity ($x_m = K_m\dot{\phi}$). However, the maximum $\dot{\phi}$ is limited by the maximum excursion of the manipulator. To ensure that the tasks corresponding to the two manipulator types have the same static gain of the controlled element, the servo-system gain K_m is set to the inverse of the static gain of the controlled element:

$$x_m = K_m \cdot \dot{\phi} = \frac{1}{K_c} \cdot \dot{\phi} \tag{2}$$

The forward gain K_f is set to one for both manipulator types. The controlled-element input u is the combination of the control signal u_p and the disturbance forcing function f_d.

1. Controlled Element

The roll dynamics of a typical wide-body jet aircraft [12] are used as the dynamics of the controlled element in the experiment. The spiral mode is simplified to a single integrator. The roll subsidence and the open-loop gain are deliberately adjusted in order to make the aircraft not too difficult to control:

$$H_c(s) = \frac{\Phi(s)}{U(s)} = \underbrace{1/(0.083s+1)}_{\text{actuator dynamics}} \cdot \underbrace{K_c \cdot (2.259s^2 + 0.821s + 1)/s(0.4s+1)(1.647s^2 + 0.336s + 1)}_{\text{aileron-to-roll-angle dynamics}} \tag{3}$$

Here, the open-loop gain (i.e., the static gain) is $K_c = 3.5$.

2. Data Collection

An experimental run lasts 90 s; during which, the subject performs the compensatory task and the data are recorded. The first 8.08 s are used as the run-in time to allow the subject to adjust to the task. The remaining 81.92 s yield the measurement data. The measurements are collected with a sampling frequency of 200 Hz. In the experiment, each subject repeated the experimental run of each condition for a number of times. The number of repetitions varied from 8 to 10, depending on how rapidly the performance converged to a stable level. The last five repetitions were used for the final analysis.

3. Forcing Functions

The two forcing functions f_t and f_d are both defined as the sum of 10 different sinusoids [13]:

$$f_t(t) = \sum_{k=1}^{10} A_t(k) \cdot \sin(\omega_t(k)t + \theta_t(k)) \tag{4}$$

$$f_d(t) = \sum_{k=1}^{10} A_d(k) \cdot \sin(\omega_d(k)t + \theta_d(k)) \tag{5}$$

Using the two forcing functions, both the pilot's reaction to the visual presentation and the response to the manipulator movement (and thus the neuromuscular impedance during the task) can be estimated [14]. To prevent participants from recognizing the signal pattern, the starting phases of the sine components are chosen randomly [15].

A lead–lag low-pass filter is selected to define the amplitudes of the forcing functions:

$$H_{\mathrm{ff}} = K_{\mathrm{ff}} \cdot \frac{(1/\omega_{\mathrm{ff},L}^2)s^2 + (2 \cdot \zeta_{\mathrm{ff}}/\omega_{\mathrm{ff},L})s + 1}{(1/\omega_{\mathrm{ff},l}^2)s^2 + (2 \cdot \zeta_{\mathrm{ff}}/\omega_{\mathrm{ff},l})s + 1} \tag{6}$$

where the gain K_{ff} and the damping ratio ζ_{ff} are 0.2 and 0.7, respectively. The amplitude of each sinusoidal component of the forcing functions is given by the magnitude of the filter at the corresponding frequency. To obtain three different forcing-function bandwidths, the two corner frequencies are adjusted, as listed in Table 2.

To keep the target-following task and the disturbance-rejection task equal in difficulty, the disturbance forcing function is adapted by scaling its magnitude with the inverse of $|H_c|$, as illustrated by Fig. 5. Details about the definition of the two forcing functions are given in Tables 3 and 4, respectively. Figure 6 gives an example of the two forcing functions with the second bandwidth (BW2). Please note that the disturbance forcing function shown in this figure is that before the adaptation.

IV. Results, Analysis, and Discussion

The measurements of the last five repetitions performed by each subject are averaged for the analysis. Comparisons between the two manipulator types are made in terms of the tracking error and the control effort, as well as the estimated open- and closed-loop frequency response functions. Twoway repeated measures analysis of variance (ANOVA) tests are performed to reveal the effects of the two independent factors. Tables 5 and 6 show the corresponding statistical results. Please note that, in the tables, MT and BW represent the manipulator type and the bandwidth, respectively.

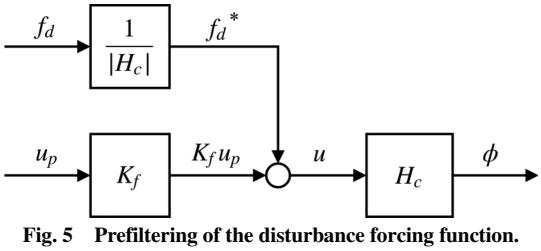

Fig. 5 Prefiltering of the disturbance forcing function.

Table 3 Target forcing function f_t

			A_t, rad			ϕ_t, rad		
k	Period	ω_t, rad/s	BW1	BW2	BW3	BW1	BW2	BW3
1	5	0.3835	0.1864	0.1984	0.1999	1.7411	2.3319	4.9089
2	11	0.8437	0.0910	0.1645	0.1944	5.4434	5.5352	0.9319
3	21	1.6107	0.0277	0.0724	0.1462	3.3194	0.6807	5.0653
4	37	2.8379	0.0094	0.0248	0.0645	3.8945	5.8910	0.4305
5	51	3.9117	0.0056	0.0134	0.0352	1.2212	3.2216	1.8187
6	71	5.4456	0.0039	0.0074	0.0185	4.3954	0.9325	5.9087
7	101	7.7466	0.0033	0.0045	0.0095	3.0397	5.6708	4.8104
8	137	10.5078	0.0032	0.0036	0.0058	0.0160	1.1480	1.8858
9	191	14.6495	0.0031	0.0032	0.0040	5.4767	4.4054	2.0951
10	224	17.1806	0.0031	0.0032	0.0036	3.4525	4.0862	1.6544

Table 4 Prefiltered disturbance forcing function f_d^*

			A_d, rad			ϕ_d, rad		
k	Period	ω_d, rad/s	BW1	BW2	BW3	BW1	BW2	BW3
1	6	0.4602	0.0242	0.0273	0.0278	1.2829	5.1081	0.4333
2	13	0.9971	0.0102	0.0213	0.0281	0.9194	4.1567	3.1062
3	23	1.7641	0.0097	0.0258	0.0557	1.8334	3.8964	0.1702
4	38	2.9146	0.0084	0.0220	0.0574	2.5865	1.1398	3.9334
5	53	4.0650	0.0090	0.0209	0.0551	1.5750	3.2806	1.2733
6	73	5.5990	0.0120	0.0221	0.0550	3.7298	3.5648	3.7481
7	103	7.9000	0.0215	0.0289	0.0599	1.5056	1.8805	3.0091
8	139	10.6612	0.0413	0.0462	0.0736	3.1201	1.6206	1.5561
9	194	14.8796	0.0934	0.0964	0.1173	1.0491	2.2507	1.9728
10	227	17.4107	0.1407	0.1430	0.1606	4.8887	4.3722	5.5454

A. Tracking Error and Control Activity

1. Tracking Error

The left plot of Fig. 7 shows the root mean square (RMS) of the error variable e (mean $\pm$ 95% confidence interval corrected for between-subject variability). As can be seen, the active manipulator leads to remarkably better performance. A twoway repeated measures ANOVA reveals significant effects of both the manipulator type and the forcing-function bandwidth on e; see Table 5. In addition, a significant interaction between these two independent factors is found. It can be readily seen from the figure that a larger improvement in performance is associated with a higher forcing-function bandwidth.

2. Control Activity

The control signals corresponding to the two manipulator types are f_m (active manipulator) and x_m (passive manipulator), respectively. A direct comparison between these two different variables may be misleading. Therefore, the control activities are evaluated on the basis of the force signals f_m, as can be seen from the right plot of Fig. 7.

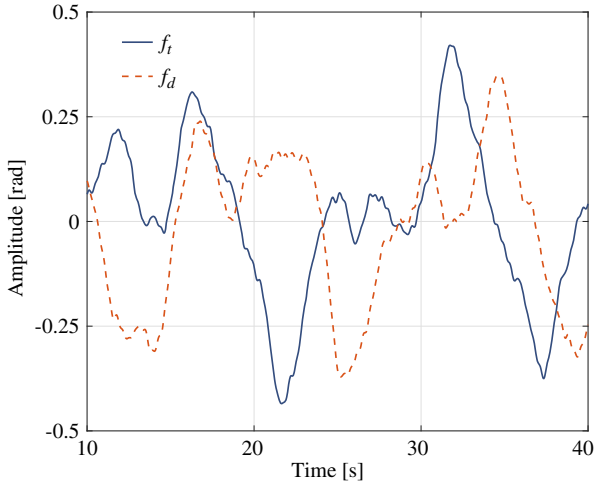

Fig. 6 Segments of the target and disturbance forcing functions: BW2.

Compared to the passive manipulator, the active manipulator leads to significant reduction in the exerted forces. The forces for both manipulator types increase significantly as a result of the extended forcing-function bandwidth. This effect is independent of the manipulator type because no interactions are found; see Table 5.

B. Frequency-Domain Analysis

In compensatory tasks with quasi-random multisine forcing functions, a human controller resembles a linear time-invariant system [16]. This allows us to estimate the frequency responses of the control loops, as well as to generalize from the findings of our study. The following subsections provide details about the frequency-domain analysis.

1. Power Spectrum of the Tracking Error

The power spectrum of the error e, corresponding to the forcing-function BW2, produced by one subject is shown in Fig. 8. Similar characteristics are observed for all other bandwidths and subjects. In the case of the passive manipulator, the magnitudes of e at the frequencies of the target and the disturbance are similar. For the active manipulator, the magnitudes that correspond to the frequencies of the target remain at roughly the same level as the passive manipulator. However, in the low-frequency region, those related to the disturbance are considerably attenuated. This demonstrates an apparent advantage of the active manipulator in rejecting the lower-frequency disturbances. Moreover, the different extents to which the error is attenuated with the active manipulator also indicate that the two tasks are accomplished with different mechanisms.

2. Open- and Closed-Loop Responses

The open- and closed-loop responses are investigated. Due to the fact that the active manipulator causes different power spectra of e at the frequencies of the target and the disturbance, the frequency responses for the two tasks are estimated separately. The open-loop frequency response of target following is obtained from the relation between e and ϕ at the frequencies of f_t:

$$H_{\mathrm{OL},t}(j\omega) = \frac{\Phi_t(j\omega)}{E_t(j\omega)} \tag{7}$$

The target-following closed-loop response is obtained by the following:

$$H_{\mathrm{CL},t}(j\omega) = \frac{\Phi_t(j\omega)}{F_t(j\omega)} \tag{8}$$

Figure 9 shows the average of the open- and closed-loop responses generated by subjects for the forcing-function BW2. Similar characteristics of the responses can be observed for the other two bandwidths. In the crossover region, the magnitudes of the open-loop responses for the two manipulator types are similar and resemble those of a single integrator, as expected by McRuer and Jex's crossover model [16]. The active manipulator leads to a smaller phase lag and a greater phase margin. This leads to a larger bandwidth, less overshoots, and smaller phase lags in the closed-loop response as compared to the passive manipulator.

The crossover frequencies ω_c and the phase margins ϕ_m of the open-loop responses averaged over all subjects are shown in Fig. 10 (mean $\pm$ 95% confidence interval corrected for between-subject variability). The results from a twoway repeated measures ANOVA suggest that the effect of the manipulator type on ω_c is significant; see Table 6. Except for the lowest forcing-function bandwidth, the active manipulator leads to a higher ω_c than the passive manipulator. The effect of the forcing-function bandwidth is also significant. For the active manipulator, ω_c remains at roughly the same level for the first two forcing-function bandwidths, and then it regresses for the highest bandwidth. For the passive manipulator, a regressing trend can be easily seen.

The effects of both independent variables on ϕ_m are found to be significant. The active manipulator leads to a significantly higher ϕ_m

Table 5 Results of ANOVA tests for tracking errors and control activities

	RMS of e			RMS of f_m		
	MT	BW	MT*BW	MT	BW	MT*BW
F value	$F(1, 11)$	$F(1.16, 12.73)$[a]	$F(2, 22)$	$F(1, 11)$	$F(2, 22)$	$F(2, 22)$
	655.2	867.9	215.9	27.72	103.4	0.405
Significance	$p < 0.05$	$p < 0.05$	$p < 0.05$	$p < 0.05$	$p < 0.05$	$p > 0.05$

[a]This F value is reported after a Greenhouse–Geisser correction.

Table 6 Results of ANOVA tests for crossover characteristics

		Crossover frequency ω_c			Phase margin ϕ_m		
		MT	BW	MT*BW	MT	BW	MT*BW
Target following	F value	$F(1, 11)$	$F(2, 22)$	$F(1.35, 14.90)$[a]	$F(1, 11)$	$F(2, 22)$	$F(1.37, 15.03)$[a]
		13.63	66.43	3.187	44.27	152.9	2.993
	Sig.	$p < 0.05$	$p < 0.05$	$p > 0.05$	$p < 0.05$	$p < 0.05$	$p > 0.05$
Disturbance rejection	F value	$F(1, 11)$	$F(2, 22)$	$F(2, 22)$	$F(1, 11)$	$F(2, 22)$	$F(2, 22)$
		298.6	4.987	43.76	14.49	17.38	2.406
	Sig.	$p < 0.05$	$p < 0.05$	$p < 0.05$	$p < 0.05$	$p < 0.05$	$p > 0.05$

[a]These F values are reported after Greenhouse–Geisser corrections.

than the passive manipulator for all three bandwidths. Also, for the active manipulator, ϕ_m remains roughly the same for the first two forcing-function bandwidths. For the highest bandwidth, subjects regressed their ω_c to increase their ϕ_m and maintain stability of the closed-loop system. The ϕ_m corresponding to the passive manipulator increases as the forcing-function bandwidth increases, as a result of crossover regression.

The open-loop frequency response of disturbance rejection is derived through the following:

$$H_{\mathrm{OL},d}(j\omega) = \frac{U_{p,d}(j\omega)}{U_d(j\omega)} \tag{9}$$

where $U_p = F_m$ in the case of the active manipulator, and $U_p = X_m$ in the case of the passive manipulator. Because the disturbance is fed into the system before the controlled element (see Fig. 5), selecting f_d^* as the input to the closed-loop system will include the aircraft dynamics in the numerator. This will make the information provided

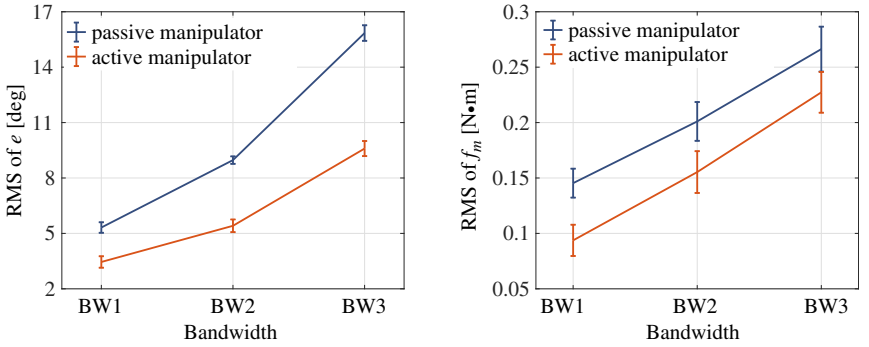

Fig. 7 RMS of the error and force signals for different conditions.

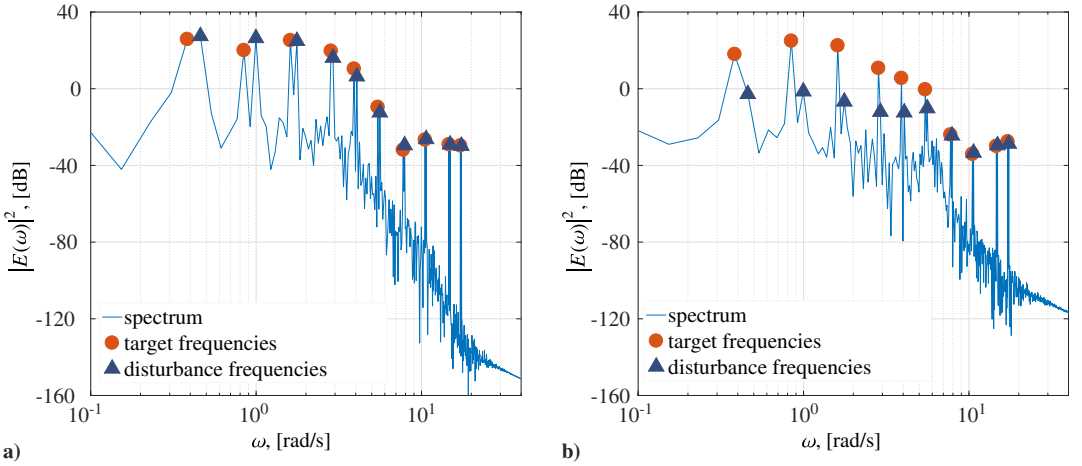

Fig. 8 Power spectra of the error $e(t)$ (one subject, BW2): a) passive manipulator; and b) active manipulator.

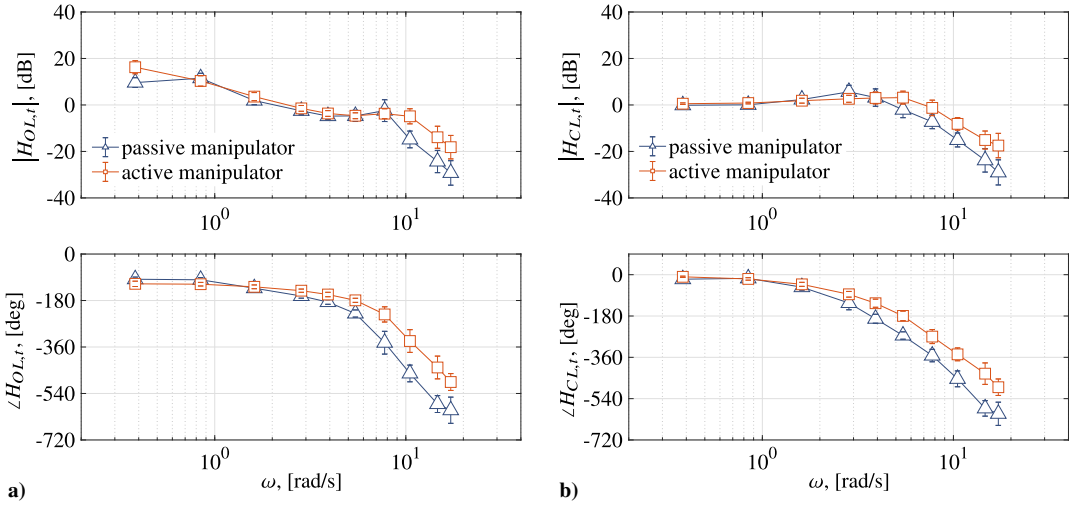

Fig. 9 Target-following frequency responses of subjects (mean ± standard deviation), BW2: a) open-loop response; b) closed-loop response.

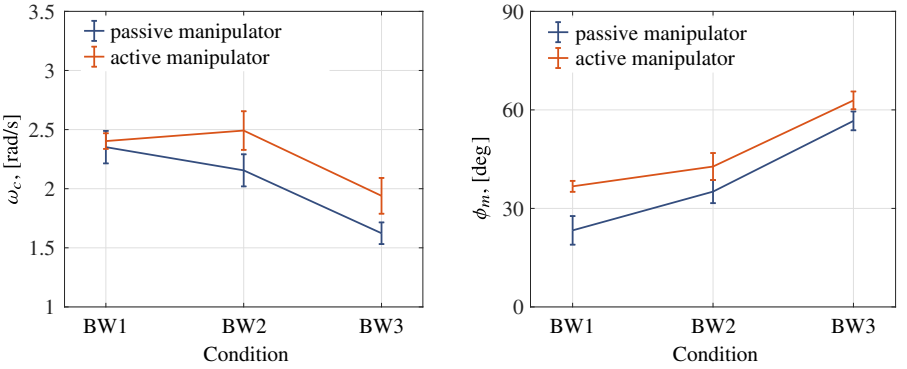

Fig. 10 Crossover characteristics of target-following open-loop responses of subjects (mean ± 95%*CI*).

by the closed-loop response not straightforward. Therefore, the following correction is made:

$$|H_{\mathrm{CL},d}(j\omega)| = \left|\frac{\Phi_d(j\omega)}{F_d^*(j\omega)}/H_c(j\omega)\right| = \left|\frac{\Phi_d(j\omega)}{F_d(j\omega)}\right|$$
$$\angle H_{\mathrm{CL},d}(j\omega) = \angle\frac{\Phi_d(j\omega)}{F_d^*(j\omega)} - \angle H_c(j\omega) \tag{10}$$

This results in the frequency response of a closed-loop system into which the disturbance is fed directly at the output of the controlled element.

Figure 11 shows the average of the open- and closed-loop frequency response estimates for all subjects for the BW2 condition. The characteristics of the frequency responses estimated for the other two bandwidths are similar. As can be seen, different manipulator types lead to notable differences in the frequency responses; the differences are much larger than those observed in target following. This is in line with that observed from the power spectrum of the error signal (see Fig. 8). The active manipulator leads to a larger open-loop gain in the crossover region. Moreover, the open-loop phase lag corresponding to the active manipulator is much smaller and remains at approximately −90 deg over the whole tested range of frequency. Therefore, the closed-loop system demonstrates significant improvements in the rejection bandwidth and produces smaller overshoots.

The crossover frequencies ω_c and phase margins ϕ_m of the open-loop responses generated by all subjects are shown in Fig. 12 (mean ± 95% confidence interval corrected for between-subject variability). As can be seen from Table 6, the effects of the manipulator type and the forcing-functions bandwidth on ω_c are significant. The interaction between these two factors is also significant, which can be expected because the two manipulator types cause the forcing-function bandwidth to have opposite effects on ω_c. For the passive manipulator, apparent crossover regression occurs. This is similar to target following, in which a declining trend of ω_c is also observed; see Fig. 10. In contrast, ω_c for the active manipulator demonstrates a notable increasing trend as the forcing-function bandwidth increases.

As a result of crossover regression, the ϕ_m corresponding to the passive manipulator increases as the bandwidth increases. Due to this, a significant effect of the forcing-function bandwidth is found. The active manipulator allows for significantly higher phase margins. In contrast to the passive manipulator, the ϕ_m with regard to the active manipulator remains roughly independent of the forcing-function bandwidth.

C. Discussion

With the passive manipulator, subjects generated very similar open-loop responses for the target-following and disturbance-rejection tasks. The crossover frequencies ω_c and the phase margins ϕ_m corresponding to these two tasks, as well as the effects of the forcing-function bandwidth, are similar. This is expected because our subjects received the information of both the target and the disturbance only through the error presented visually. Consequently, their actions for these two tasks must be similar.

In general, the active manipulator leads to a pronounced performance improvement. It seems that a greater improvement is associated with higher task difficulty (the higher forcing-function bandwidths). An interesting fact associated with the active manipulator is that a clear distinction exists in the open-loop frequency response between target following and disturbance rejection, as well as in the characteristics of ω_c and ϕ_m. Disturbance rejection possesses higher open-loop gains and smaller phase lags than target following. Moreover, crossover regression occurs in target following in the case of the highest forcing-function bandwidth. However, the crossover frequency of the disturbance-rejection loop does not regress; instead, it increases when the forcing-function bandwidth increases.

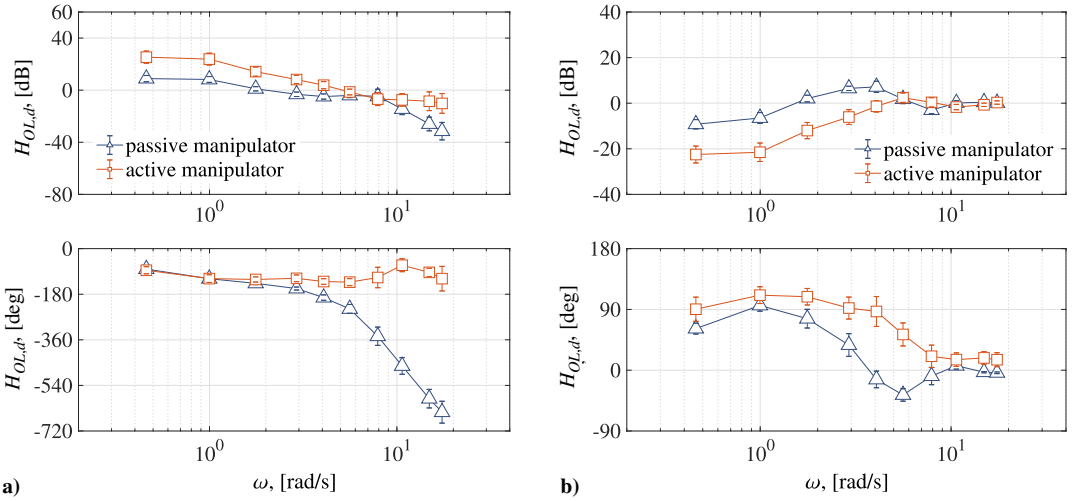

Fig. 11 Disturbance-rejection frequency responses of subjects (mean ± std) with BW2: a) open-loop response; and b) closed-loop response.

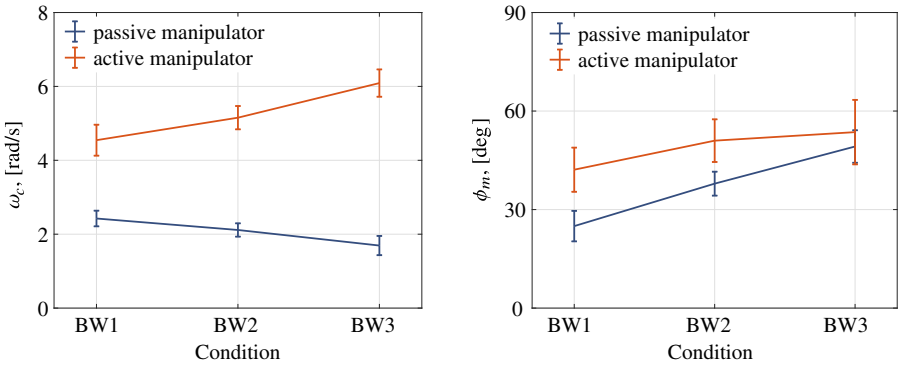

Fig. 12 Crossover characteristics of disturbance-rejection open-loop responses of subjects (mean ± 95%*CI*).

This remarkable difference indicates that, with the active manipulator, following the target and rejecting the disturbance are accomplished independently, although these two tasks are performed simultaneously. This is likely caused by the fact that subjects can benefit from the haptic feedback of the aircraft rotational velocity. The neuromuscular system that controls the movement of the manipulator may play a more important role in controlling the aircraft state. This hypothesis will be further explored in the following section.

V. Mechanism of Aircraft Control with the Active Manipulator

The mechanism of controlling the aircraft with the active manipulator can be presented more intuitively by means of a two-port network representation [17,18], as can be seen in Fig. 13. Please note that the disturbance f_d and the forward gain K_f are omitted here for the reason of simplicity. In addition, the arrow under $K_m\dot{\phi}$ indicates the direction of the energy flow, which is not necessarily the direction of the transmission of ϕ [18].

We assume that the sampling and the servo system have negligible effects on the overall dynamics in the frequency range of interest. In this case, the force sensor and the servo system act as transparent mediums that directly connect the pilot to the aircraft. When the pilot applies a force on the manipulator, a change occurs in the aircraft rotational velocity. The manipulator moves at the same moment, as if it is moved by the pilot directly. In other words, when the pilot moves the manipulator, the rotational velocity of the aircraft exhibits exactly the same changes. One can imagine that the pilot still controls the aircraft attitude by means of the manipulator deflection, as he/she does with the passive manipulator. The dynamics of the manipulator become the dynamics that correspond to the aircraft rotational velocity in response to the aircraft input:

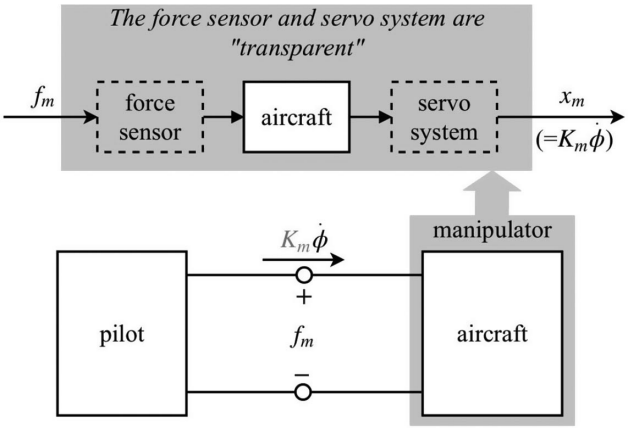

Fig. 13 Two-port representation [17,18] of the pilot-manipulator system.

$$H_{m,a} = \frac{X_m(s)}{F_m(s)} = K_m \cdot s \cdot \frac{\Phi(s)}{U(s)} = K_m \cdot sH_c(s) \tag{11}$$

Then, independent of the aircraft dynamics, the dynamics of the effective controlled element always become a single integrator:

$$H_{c,\text{eff}} = \frac{\Phi(s)}{X_m(s)} = \frac{1}{K_m} \cdot \frac{1}{\text{s}} \tag{12}$$

The observed improvement in target following can therefore be explained by the simplification of the controlled element, as expected by McRuer and Jex's crossover model [16]. Moreover, it is readily

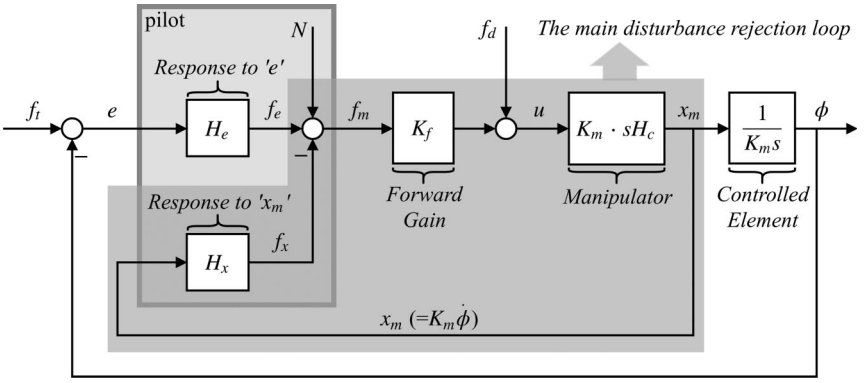

Fig. 14 Schematic diagram in which the pilot is represented by two subsystems.

appreciable that the disturbance acting on the aircraft becomes the disturbance to the manipulator. Rejection of the disturbance can then be easily achieved by stabilizing the manipulator position. With the active manipulator, this task is integrated into the neuromuscular system, and it becomes largely independent of the elimination of the visual error e. This explains the distinction in the response between target following and disturbance rejection.

To understand the effects of the forcing-function bandwidth on disturbance rejection, the impedance of the neuromuscular system of our subjects is estimated. Here, the term "impedance" is defined as a measure of how much the human arm "resists" a disturbance motion. To this end, the pilot dynamics are first represented by three components, as shown by Fig. 14.

The pilot force f_m is divided into three components, i.e., f_x, f_e, and N. The first two variables are the outputs of two internal systems H_x and H_e, and the last one accounts for any nonlinearity of the pilot dynamics. Assume for the moment that this remnant N is small as compared to f_e and f_x; then, the dynamics of the pilot can be accurately described by the two internal systems. The system H_x generates the force component in response to the movement of the manipulator, and it indicates the mechanical impedance of the neuromuscular system [14]. Due to the fact that the energy of the error signal e can be considered to be small at the frequencies of the disturbance (see Fig. 8b), disturbance rejection is mainly accomplished by the loop that is shaded in Fig. 14. In this case, the neuromuscular impedance H_x becomes the dynamic gain of the feedback path. This indicates that a greater magnitude of H_x (a higher impedance, i.e., more resistance to changing stick deflections) will lead to better rejection of the disturbance.

The remainder of the pilot dynamics (including the pilot adaptation behavior, the internal representation, the neural filters, and so forth [14]) is accounted for by H_e. This system, which generates the force in response to the visually presented error signal, is used in this study as an intermediate variable for separating H_x from the dynamics of the pilot. Readers are referred to the work by van Paassen et al. [14,19] for greater detail about these two internal systems.

Figure 15 shows the bode plot of the estimated H_x for the three bandwidths considered. The characteristics of H_x are consistent with the findings shown earlier (see Fig. 12). In general, higher forcing-function bandwidths lead to higher magnitudes of the impedance $|H_x|$. In the crossover region, the increase in $|H_x|$ increases the open-loop gain. As a result, the crossover frequency ω_c increases as the forcing-function bandwidth increases. The increase in magnitude indicates that our subjects stiffened their arms when the disturbance on the manipulator became stronger. This is indeed confirmed by an interview carried out after the experiment with our subjects.

The phase characteristics corresponding to the three bandwidths are similar. In the crossover region, the phase lags ($\angle H_x$) under the three conditions are approximately the same. This explains why no significant changes in the phase margin ϕ_m were found.

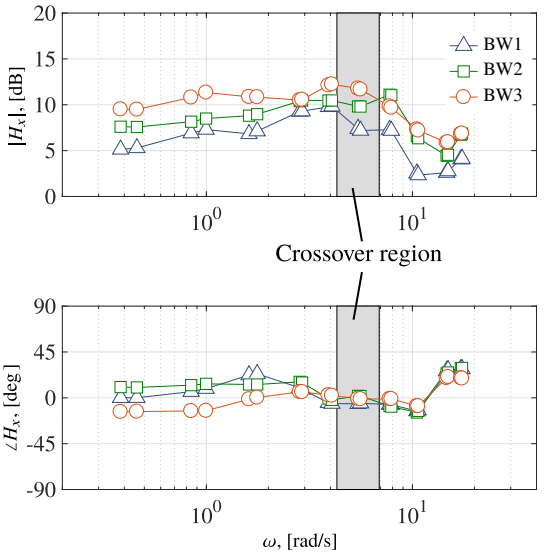

Fig. 15 Subjects' average neuromuscular impedance corresponding to the three forcing-function bandwidths.

VI. Improving the Active Manipulator

The current configuration of the active manipulator feeds back the aircraft rotational rate with its full spectrum. As a result, the effects of the high-frequency components of the disturbance acting on the aircraft are also presented to the pilot. As can be seen from Figs. 8 and 11, humans only have limited bandwidth for disturbance rejection. The components of the disturbance beyond the bandwidth are still present in the movement of the manipulator, leading the pilot's arm to involuntarily move with the manipulator. During the experiment, many subjects indicated that this involuntary movement was intrusive and reduced the operational relevance of the active manipulator.

To provide better operational quality, we designed a low-pass filter, placed before the servo system, which is illustrated in Fig. 16.

When the low-pass filter $H_{\text{lpf}}(s)$ is implemented, the manipulator deflection can be expressed as follows:

$$X_m(s) = K_m \cdot s \cdot \Phi(s) \cdot H_{\text{lpf}}(s) \tag{13}$$

In this case, the manipulator dynamics become the following:

$$H_{m,\text{af}} = \frac{X_m(s)}{U(s)} = K_m \cdot sH_c(s) \cdot H_{\text{lpf}}(s) \tag{14}$$

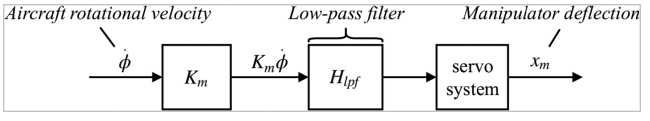

Fig. 16 Configuration of the active manipulator with a low-pass filter.

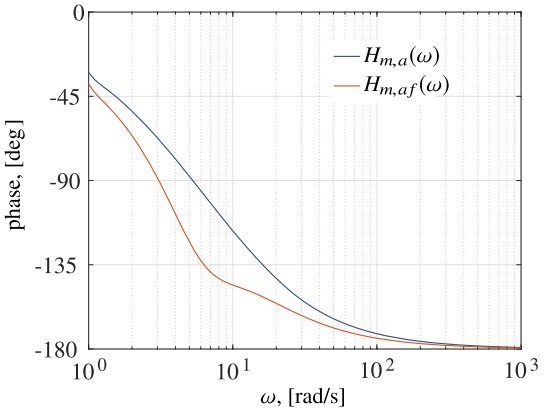

Fig. 17 Phase characteristics of the active manipulator with/without the lead–lag filter.

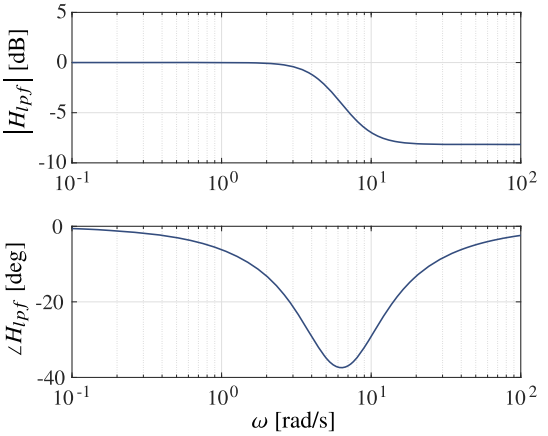

Fig. 18 Bode plot of the lead–lag filter.

The pilot still directly perceives the aircraft rotational velocity through the manipulator, but now within the passband of H_{lpf}. The aircraft rotational motion that lies within the stopband of the filter is no longer present in the movement of the manipulator. On the one hand, the filter H_{lpf} should sufficiently filter out the high-frequency disturbance that is beyond human capability. On the other hand, the filter should not deteriorate the dynamics of the effective controlled element. A properly designed filter should attenuate the energy of the disturbance that lies beyond the crossover region of the disturbance-rejection response while maintaining the dynamics of the controlled element as a single integrator in the crossover region of the target-following response; see Eq. (12).

In addition, the original passivity properties of the manipulator should be preserved to maintain the stable interaction between the pilot and the aircraft [18,20–22]. In our case, this is equivalent to avoiding causing the phase lag of the manipulator dynamics to exceed −180 deg. Due to the dynamics of the aircraft [see Eq. (3)], any additional phase lag at high frequencies will cause the manipulator to lose the passivity (see Fig. 17) and may lead to an unstable haptic interaction [21]. Therefore, a lead–lag filter with the following dynamics is designed:

$$H_{\text{lpf}} = \frac{\omega_{\text{lpf},l}^2}{\omega_{\text{lpf},L}^2} \cdot \frac{s^2 + 2\zeta_{\text{lpf}} \cdot \omega_{\text{lpf},L} + \omega_{\text{lpf},L}^2}{s^2 + 2\zeta_{\text{lpf}} \cdot \omega_{\text{lpf},l} + \omega_{\text{lpf},l}^2} \tag{15}$$

where $\omega_{\text{lpf},l} < \omega_{\text{lpf},L}$, and $\zeta_{\text{lpf}} = 0.7$.

The first corner frequency can be selected based on the findings from the experiment. As can be seen from Fig. 12, the crossover frequency ω_c for disturbance rejection lies in the range of 4.5 to 6.1 rad/s. The higher end of this range corresponds to a high level of the neuromuscular impedance that, according to our experimental participants, caused considerable muscle fatigue. The impedance levels that correspond to the two lower values of ω_c were considered by our participants to be satisfactory. Therefore, in this study, we set $\omega_{\text{lpf},l} = 5$ rad/s, which is a value that is also sufficiently higher than the crossover frequency of the target-following response. With this setting, we expect the target-following performance to remain the same [16].

To preserve the passivity of the manipulator, we set $\omega_{\text{lpf},L} = 8$ rad/s. Figure 17 shows the phase characteristics of the manipulator with this filter. As can be seen, the passivity of the manipulator is maintained at high frequencies. Thus, the stability of the interaction between the pilot and the aircraft is guaranteed. More important, the information of the aircraft state is well preserved within the target-following bandwidth, whereas that beyond the disturbance-rejection bandwidth is largely attenuated by 60%, as shown by Fig. 18.

VII. Experiment Two: Testing the Lead–Lag Filter

A. Experiment Design

To evaluate the new configuration of the active manipulator, we carried out a second experiment with four participants. The experimental task is again target-following and disturbance-rejection compensatory tracking. The setups of the two forcing functions, f_t and f_d, are the same as the BW2 condition used in the first experiment, as shown in Tables 3 and 4. All remaining setups of the experiment including the controlled-element dynamics, the duration of each experimental run, the data collection, the experimental devices, and so forth are the same as the first experiment.

The new configuration of the active manipulator will be compared with the original one (used in the first experiment). To reduce the increase caused by the filter in the mechanical impedance of the manipulator, the forward gain K_f (see Figs. 1b and 3b) is set to 2.5. This gain of the original setup is set to the same value for a fair comparison.

B. Results

As mentioned earlier, the selected filter is able to reduce the high-frequency components of the disturbance by approximately 60%. Due to this, during the experiment, our subjects barely noticed any involuntary arm movements. Furthermore, the lead–lag filter did not affect the task performance, as can be seen in Fig. 19, which presents the RMS of the error signal e (mean $\pm$ 95% confidence interval corrected for between-subject variability). The result from a dependent t-test suggests that the tracking errors corresponding to the two manipulator setups are comparable [$t(3) = -0.745$, $p > 0.05$].

Figure 20 presents the open- and closed-loop frequency responses of target following generated by our subjects. As can be seen, the two configurations lead to approximately the same frequency responses. Figure 21 shows the crossover frequency ω_c and the phase margin ϕ_m (mean $\pm$ 95% confidence interval corrected for between-subject variability).

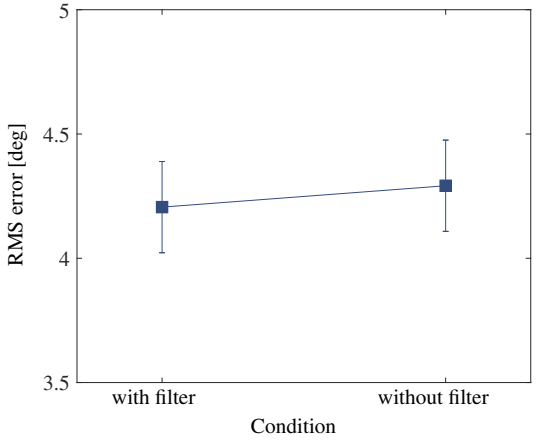

Fig. 19 Root mean square of the error signals produced by subjects (mean ± 95%CI).

Dependent t tests reveal that the ω_c and ϕ_m corresponding to the two configurations are approximately the same [$t(3) = -2.643$, $p > 0.05$ for ω_c and $t(3) = 1.962$, $p > 0.05$ for ϕ_m]. This confirms that the lead–lag filter does not affect the target-following performance of our subjects and that the equivalent controlled-element dynamics still approximate to a single integrator.

Figure 22 shows the open- and closed-loop frequency responses of disturbance rejection. In general, the two configurations result in similar responses. The open-loop gain is not affected by the lead–lag filter, and it still possesses the characteristics of a single integrator. As a result, the closed-loop bandwidths for the two manipulator configurations are approximately the same. However, the lead–lag filter leads to a larger open-loop phase lag at the crossover region.

The ω_c and ϕ_m of the disturbance-rejection responses that correspond to the two manipulator configurations are presented in Fig. 23 (mean ± 95% confidence interval corrected for between-subject variability). As expected, the two configurations lead to similar ω_c, as suggested by the result of a dependent t test: $t(3) = 2.206$, $p > 0.05$. However, the lead–lag filter caused a significant reduction of about 40 deg in ϕ_m [$t(3) = -7.981$, $p < 0.05$].

This reduction in the phase margin is due to the phase lag introduced by the lead–lag filter. As can be seen from Fig. 18, the filter introduces roughly the same amount of the phase lag at the crossover region, which is approximately 40 deg, Nevertheless, this reduction in ϕ_m does not affect the performance of our subjects. The remaining phase margin of around 30 deg still guarantees a good closed-loop response.

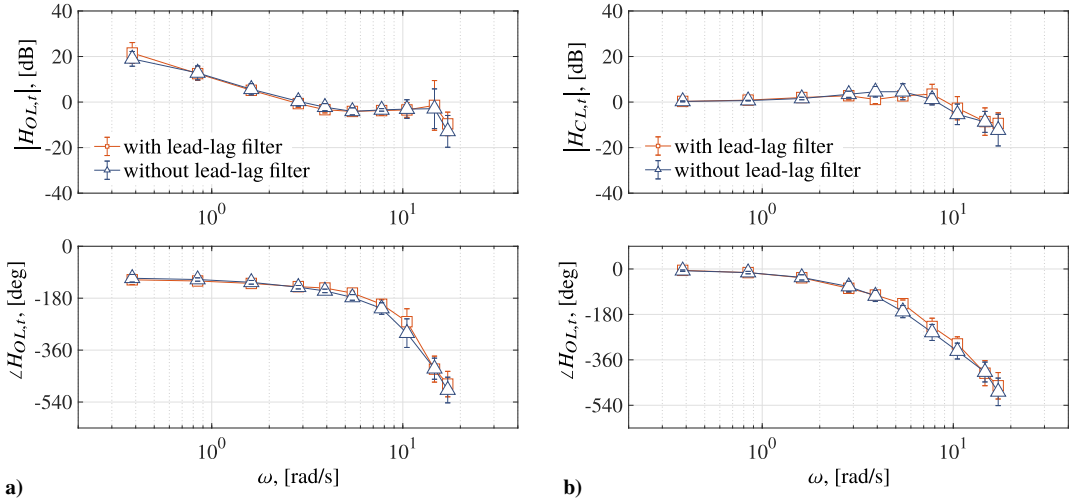

Fig. 20 Target-following frequency responses of subjects (mean ± std): a) open-loop response; and b) closed-loop response.

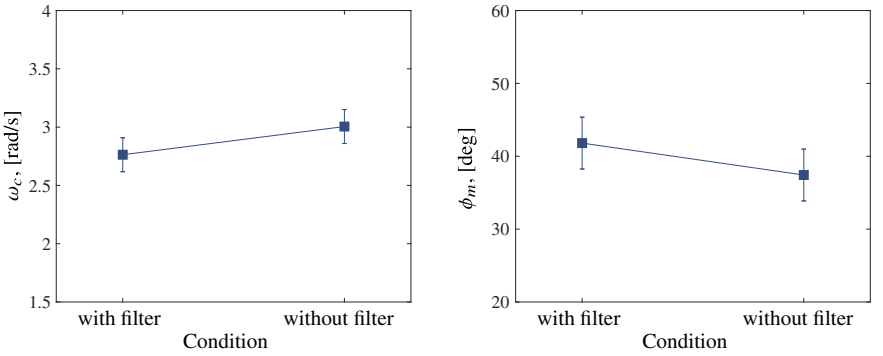

Fig. 21 Crossover frequencies and phase margins of target-following responses (mean ± 95%*CI*).

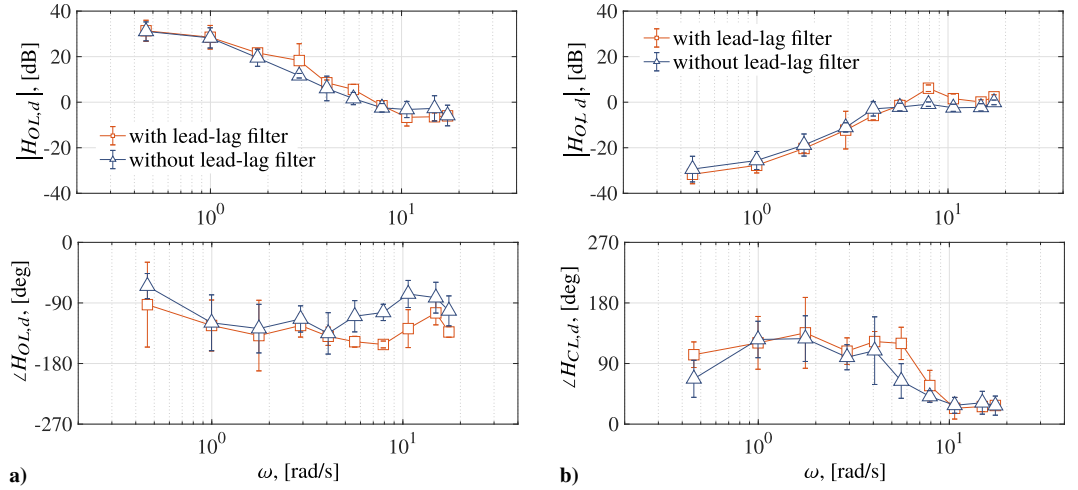

Fig. 22 Disturbance-rejection frequency responses of subjects (mean ± std).

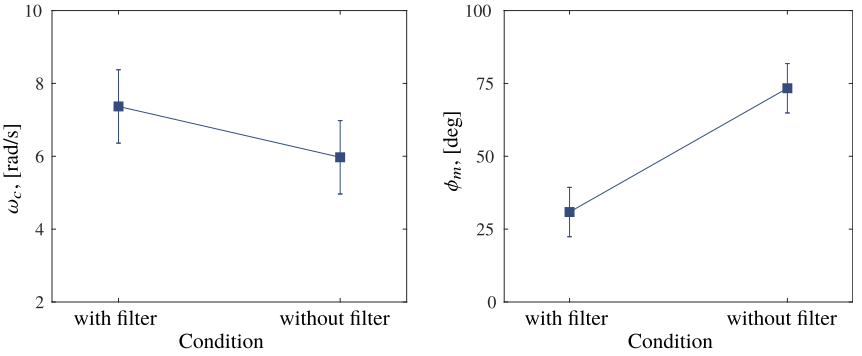

Fig. 23 Crossover frequencies and phase margins of the disturbance-rejection responses (mean ± 95%*CI*).

VIII. Discussion

In this study, we first revisited the active manipulator proposed in previous work [9,10]. The observed improvement in the task performance is similar to the previous findings: except that, in the previous work, the effect of the manipulator type on the disturbance-rejection phase margin was not significant. However, this is probably due to the fact that the forcing functions used in our current work are different. As discussed in Sec. IV, the difference in ϕ_m between the two manipulator types may vary with different forcing-function bandwidths (see Fig. 12). Another possible reason lies in the number of subjects. In the previous work, only two subjects participated in the experiment, which may not be sufficient for the elimination of individual variations. In our current work, 12 subjects were invited, which would lead to a more generalized and reliable conclusion.

The control input to the aircraft in the case of the active manipulator is the pilot's force instead of the manipulator deflection, as in the case of the passive manipulator. Although the control inputs are different, the control processes associated with the two manipulator types are in fact similar, a process achieved by means of the manipulator deflection. As shown by the analysis in Sec. V, the control input to the effective controlled element in the case of the active manipulator is still the manipulator deflection. In addition, our previous study shows that pilots can perform control tasks much better with an active manipulator than an isometric (force) control device [10]. One can imagine that the performance improvement associated with the active manipulator is due to the haptic feedback instead of the change in the control input.

With the feedback about the rotational velocity, the active manipulator leads to a more pronounced improvement as the difficulty of the task increases. This is due to the fact that the active manipulator simplifies the dynamics of the controlled element into a single integrator, independent of the aircraft dynamics. Furthermore, the rejection of the disturbance is integrated into the coupled neuromuscular-manipulator system. This allows one to haptically perform the disturbance-rejection task separately from the (predominantly visual) target-following task. With an active manipulator, regulating the aircraft states is largely allocated to the cerebellum, which is responsible for the control of limb movements [23,24]. The workload of the cerebrum, which is responsible for the equalization of visual presentation, is therefore reduced. In addition, the haptic feedback more effectively involves spinal reflexes and muscle cocontraction in rejecting the disturbance acting on the aircraft, allowing for much faster and more robust responses [25].

According to our subjects, the high-frequency components of the disturbance acting on the aircraft reduced the operational quality of the active manipulator. We successfully mitigated this effect by means of a lead–lag filter, which was tested in the second experiment. Note that, in practice, the dynamics of the aircraft may be (slowly) time varying, depending on the current flight conditions, like altitude and speed. This entails adjusting the lead coefficient of the filter according to different equilibrium conditions. The passband of the filter should also be adjusted using the data collected from pilots and the power spectrum of the actual disturbance, as well as the highest neuromuscular impedance, which does not lead to considerable physical fatigue.

This study, in line with previous studies into active manipulators, used unaugmented aircraft dynamics. However, there is no reason why an active manipulator cannot be combined with an aircraft equipped with a stability or control augmentation system, given that one evaluates the effective dynamics of the manipulator to be compatible with control by the neuromuscular system. An additional advantage of such a setup would be that pilots could also feel, through the manipulator, the effect of any flight envelope protection systems [26] or the actions of the autopilot. The current study only evaluated the feedback of aircraft attitude rate on the stick. Rate feedback is a sensible choice because it leads the effective controlled element to become a single integrator, which is known to result in high performance and low workload. Furthermore, the second experiment demonstrates that a filtered feedback system is also appropriate. This creates further possibilities for optimizing the effective manipulator dynamics according to the mechanical characteristics perceived by the pilot [27,28].

IX. Conclusions

This study presents a new evaluation of a haptic interface for aircraft control. The proposed haptic interface, termed the active manipulator, feeds back the aircraft rotational rate through the manipulator defection angle. The results from a first target tracking and disturbance-rejection experiment indicate that the active manipulator leads to a significant improvement in task performance as compared to the passive manipulator. A theoretical analysis shows that the active manipulator simplifies the dynamics of the controlled element into a single integrator, independent of the actual aircraft dynamics. It is also shown that the disturbance-rejection part of the task is effectively integrated into the neuromuscular system, and it becomes largely independent of the target-following part of the task.

High-frequency components of the disturbance signal result in involuntary arm movements that reduce the operational effectiveness of the active manipulator. A lead–lag filter is developed and tested in a second experiment. The results show that the implementation of the low-pass filter leads to comparable task performance, and it considerably improves the operational quality of the active manipulator.

References

[1] Ferrell, W. R., "Delayed Force Feedback," *Human Factors*, Vol. 8, No. 5, 2016, pp. 449–455. doi:10.1177/001872086600800509

[2] Anderson, R. J., and Spong, M. W., "Bilateral Control of Teleoperators with Time Delay," *IEEE Transactions on Automatic Control*, Vol. 34, No. 5, 1989, pp. 494–501. doi:10.1109/9.24201

[3] Niemeyer, G., and Slotine, J. J., "Stable Adaptive Teleoperation," *IEEE Journal of Oceanic Engineering*, Vol. 16, No. 1, 1991, pp. 152–162. doi:10.1109/48.64895

[4] Ryu, J. H., Kwon, D. S., and Hannaford, B., "Stable Teleoperation with Time-Domain Passivity Control," *IEEE Transactions on Robotics and Automation*, Vol. 20, No. 2, 2004, pp. 365–373. doi:10.1109/TRA.2004.824689

[5] Lam, T. M., Mulder, M., and Van Paassen, M. M., "Haptic Feedback in Uninhabited Aerial Vehicle Teleoperation with Time Delay,"

Journal of Guidance, Control, and Dynamics, Vol. 31, No. 6, 2008, pp. 1728–1739.
doi:10.2514/1.35340

[6] Hirche, S., Matiakis, T., and Buss, M., "A Distributed Controller Approach for Delay-Independent Stability of Networked Control Systems," *Automatica*, Vol. 45, No. 8, 2009, pp. 1828–1836.
doi:10.1016/j.automatica.2009.04.016

[7] Mulder, M., Abbink, D. A., Van Paassen, M. M., and Mulder, M., "Design of a Haptic Gas Pedal for Active Car-Following Support," *IEEE Transactions on Intelligent Transportation Systems*, Vol. 12, No. 1, 2011, pp. 268–279.
doi:10.1109/TITS.2010.2091407

[8] De Stigter, S., Mulder, M., and Van Paassen, M. M., "Design and Evaluation of a Haptic Flight Director," *Journal of Guidance, Control, and Dynamics*, Vol. 30, No. 1, 2007, pp. 35–46.
doi:10.2514/1.20593

[9] Hosman, R. J. A. W., Benard, B., and Fourquet, H., "Active and Passive Side Stick Controllers in Manual Aircraft Control," *Proceedings of the 1990 IEEE International Conference on Systems, Man and Cybernetics (SMC)*, IEEE Publ., Piscataway, NJ, 1990, pp. 527–529.
doi:10.1109/ICSMC.1990.142165

[10] Hosman, R. J. A. W., and Van Der Vaart, J. C., "Active and Passive Side Stick Controllers: Tracking Task Performance and Pilot Control Behavior," *Proceedings of the AGARD Conference on the Man-Machine Interface in Tactical Aircraft Design and Combat Automation*, AGARD CP 425, Neuilly-Sur-Seine, France, 1988, pp. 26-1–26-11.

[11] Adams, R. J., and Hannaford, B., "Stable Haptic Interaction with Birtual Environments," *IEEE Transactions Robotics and Automation*, Vol. 15, No. 3, 1999, pp. 465–474.
doi:10.1109/70.768179

[12] Heffley, R. K., and Jewell, W. F., "Aircraft Handling Qualities Data," NASA CR-2144, Dec. 1972.

[13] Van Paassen, M. M., and Mulder, M., "Identification of Human Control Behavior," *International Encyclopedia of Ergonomics and Human Factors*, 2nd ed., edited by W. Karwowski, Taylor and Francis, London, 2006, pp. 400–407.

[14] Van Paassen, M. M., Van Der Vaart, J. C., and Mulder, J. A., "Model of the Neuromuscular Dynamics of the Human Pilot's Arm," *Journal of Aircraft*, Vol. 41, No. 6, 2004, pp. 1482–1490.
doi:10.2514/1.14434

[15] Damveld, H. J., Beerens, G. C., Mulder, M., and Van Paassen, M. M., "Design of Forcing Functions for the Identification of Human Control Behavior," *Journal of Guidance, Control, and Dynamics*, Vol. 33, No. 4, 2010, pp. 1064–1081.
doi:10.2514/1.47730

[16] McRuer, D. T., and Jex, H. R., "A Review of Quasi-Linear Pilot Models," *IEEE Transactions on Human Factors in Electronics*, Vol. HFE-8, No. 3, 1967, pp. 231–249.
doi:10.1109/THFE.1967.234304

[17] Hannaford, B., "A Design Framework for Teleoperators with Kinesthetic Feedback," *IEEE Transactions on Robotics and Automation*, Vol. 5, No. 4, 1989, pp. 426–434.
doi:10.1109/70.88057

[18] Haykin, S. S., *Active Network Theory*, Vol. 2680, Addison-Wesley, Reading, MA, 1970, pp. 77–259.

[19] Van Paassen, M. M., "Biophysics in Aircraft Control: a Model of the Neuromuscular System of the Pilot's Arm," Ph.D. Thesis, Delft Univ. of Technology, Delft, The Netherlands, 1994, pp. 155–192.

[20] Colgate, J. E., and Hogan, N., "The Interaction of Robots with Passive Environments: Application to Force Feedback Control," *Proceedings of the 4th International Conference on Advanced Robotics Columbus*, Springer, Berlin, 1989, pp. 465–474.
doi:10.1007/978-3-642-83957-3_33

[21] Colgate, J. E., "Coupled Stability of Multiport Systems—Theory and Experiments," *Journal of Dynamic Systems, Measurement, and Control*, Vol. 116, No. 3, 1994, pp. 419–428.
doi:10.1115/1.2899237

[22] Hannaford, B., and Ryu, J.-H., "Time-Domain Passivity Control of Haptic Interfaces," *IEEE Transactions on Robotics and Automation*, Vol. 18, No. 1, 2002, pp. 1–10.
doi:10.1109/70.988969

[23] Wolpert, D. M., and Ghahramani, Z., "Computational Principles of Movement Neuroscience," *Nature Neuroscience*, Vol. 3, Nov. 2000, pp. 1212–1217.
doi:10.1038/81497

[24] Kawato, M., "Internal Models for Motor Control and Trajectory Planning," *Current Opinion in Neurobiology*, Vol. 9, No. 6, 1999, pp. 718–727.
doi:10.1016/S0959-4388(99)00028-8

[25] Abbink, D. A., "Neuromuscular Analysis of Haptic Gas Pedal Feedback During Car Following," Ph.D. Thesis, Delft Univ. of Technology, Delft, The Netherlands, 2006, pp. 1–16.

[26] Van Baelen, D., Ellerbroek, J., Van Paassen, M. M., and Mulder, M., "Design of a Haptic Feedback System for Flight Envelope Protection," *2018 AIAA Modeling and Simulation Technologies Conference*, AIAA Paper 2018-0117, 2017.
doi:10.2514/6.2018-0117

[27] Fu, W., Van Paassen, M. M., Abbink, D. A., and Mulder, M., "Framework for Human Haptic Perception with Delayed Force Feedback," *IEEE Transactions on Human-Machine Systems*, Vol. 49, No. 2, April 2019, pp. 171–182..
doi:10.1109/THMS.2018.2885401

[28] Fu, W., Landman, A., Van Paassen, M. M., and Mulder, M., "Modeling Human Difference Threshold in Perceiving Mechanical Properties from Force," *IEEE Transactions Human-Machine Systems*, Vol. 48, No. 4, 2018, pp. 359–368.
doi:10.1109/THMS.2018.2844212